Advanced battery management system design for SOC/SOH estimation for e-bikes applications

Carlo Taborelli and Simona Onori*

Department of Automotive Engineering,
Clemson University,
4 Research Drive, Greenville, SC 29607, USA
Email: c.taborelli@gmail.com
Email: sonori@clemson.edu
*Corresponding author

Sebastien Maes, Peter Sveum and Said Al-Hallaj

AllCell Technologies,
2321 W. 41st St., Chicago, IL 60609, USA
Email: smaes@allcelltech.com
Email: psveum@allcelltech.com
Email: salhallaj@allcelltech.com

Naz Al-Khayat

NRG Renew LLC,
4900 N. Scottsdale Road,
Suite 5000 Scottsdale, AZ 85251
and
AllCell Technologies,
2321 W. 41st St., Chicago, IL 60609, USA
Email: Nazar.Al-Khayat@nrg.com

Abstract: In this work, state of charge (*SOC*) and state of health (*SOH*) estimation algorithms for battery management system are proposed and compared. These algorithms are developed on a battery pack designed specifically for light electric vehicle (electric scooter or bicycles) applications. The advanced battery management system is designed in order to evaluate the instantaneous charge available in the battery and at the same time to monitor the slowly varying battery aging parameters. Two *SOC* estimation algorithms are proposed: an extended Kalman filter (EKF) and an adaptive extended Kalman filter (AEKF). With the adaptive version of Kalman filter a proper value of the model noise covariance is adaptively set using the information coming from the online innovation analysis. In the second part of this paper, a new estimation algorithm based on least squares is proposed to estimate the battery *SOH*. A general framework for a combined evaluation of *SOC*/*SOH* is discussed.

Keywords: estimation; battery; Kalman filter; e-bike; battery management system; BMS; state-of-charge; SOC; state-of-health; SOH; electric powertrain.

Biographical notes: Carlo Taborelli received his MSc in Automation Engineering at Politecnico di Milano in December 2013. He is discussing a thesis about developing a stabilising control strategy for a 4-wheeled tilting vehicle designed by Piaggio, using differential torque provided by in-wheel electric motors. From January 2014 to October 2014 he joined Clemson University-International Center for Automotive Research (CU-ICAR), Greenville, SC (USA) as a visiting scholar working on estimation algorithms and battery modelling and identification for vehicle application. At present he works as Control Engineer at Indeva s.p.a, Brembilla (BG – Italy), developing control strategies and embedded firmware for automatic guided vehicle (AGV) application.

Simona Onori received her Laurea degree, summa cum laude, (CSE) in 2003, her MS (ECE) in 2004, her PhD (Control Engineering) in 2007, from University of Rome 'Tor Vergata', University of New Mexico, USA, and University of Rome 'Tor Vergata', respectively. Prior to joining the Clemson University faculty in August 2013, she was a Research Scientist at the Ohio State University. She works on modelling, simulation, optimisation and control for advanced powertrain systems, and aging, characterisation, modelling and identification of batteries (Li-ion and PbA) for state of health estimation and remaining useful life prediction. Her research has been funded, among others, by Honda R&D Japan, Ford, GM, Cummins, NSF and US-DOE. She is a member of IEEE, ASME and SAE.

Sebastien Maes works at AllCell Technologies as an Embedded Electrics Engineer. His work has been dedicated to the safe operation and optimal performance of lithium-ion batteries through his efforts designing a battery management system technology platform and its algorithms including the Kalman filter-based state of charge estimation. He graduated in France from ENSEA (Cergy) with a Master of Science in Electrical Engineering, and a specialty in embedded systems.

Peter Sveum serves as Director of Engineering for AllCell Technologies. He has led the design of numerous fully integrated battery systems from portable units to grid scale battery offerings. In addition, he has contributed heavily to the company's proprietary battery management system development and published several peer reviewed papers. He holds an ME in Electrical Engineering as well as a BS in both Computer and Electrical Engineering from the Illinois Institute of Technology (IIT).

Said Al-Hallaj is the CEO and co-founder of All Cell Technologies LLC, and a Visiting Research Professor of Chemical Engineering at the University of Illinois at Chicago (UIC). He earned his BSc and MSc in Chemical Engineering from Jordan University of Science and Technology (JUST) and his PhD in Chemical Engineering from the Illinois Institute of Technology (IIT). He co-authored a book entitled *Hybrid Hydrogen Systems* and has published over 40 peer reviewed journal papers. He is the co-author of several issued patents and patent applications in the areas of renewable energy, energy storage and conversion and water desalination.

Naz Al-Khayat is an accomplished engineering leader with over 25 years of product and industrial process development. He has more than 40 publications and 20 patents covering powertrain, electrical machines and power electronics.

> **Comment [t1]:** Author: Please confirm if the pronoun used is correct.

He is a specialist in the design, analysis and development of powertrain or systems and associated controls. He has ten years of DFSS/TDFSS experience as a certified belt delivering savings and product development tools for new product and manufacturing process improvement.

This paper is a revised and expanded version of a paper entitled 'State of charge estimation using extended Kalman filters for battery management system', presented at 2014 IEEE International Electric Vehicle Conference, Florence, Italy, 17–19 December 2014.

1 Introduction

Light electric vehicles, such as electric bikes (e-bike) or scooters, offer many benefits over their traditional counterparts as they can go further than conventional bicycles with little effort. They can be quickly recharged anywhere a power supply is available, or low (in state of charge – *SOC*) batteries can be swapped in no time instantly with fully charged batteries.

Lithium-ion batteries have become the battery of choice not only for hybrid and electric cars, but also for electric bicycle and scooter applications. The key drivers are their high specific energy, energy density, cycle/calendar life as well as their reduced need for maintenance as compared to flooded lead acid batteries.

As technology advances, batteries are now also required to communicate with other components within the vehicle such as the motor controller to maximise range and acceleration. An accurate estimation of the energy available inside the battery is essential to optimise powertrain operation and prevent stranding the rider. Lastly, knowing the remaining energy also helps prevent overcharge and over discharge of batteries, vital to safe use and long life of lithium-ion batteries.

The battery *SOC* is generally used as a metric to quantify the amount of energy left in a battery compared with the energy it had when it was full and it gives the user an indication of how much longer a battery will continue to perform before it needs recharging. Battery state of health (*SOH*), on the other hand, represents the level of degradation of the battery due to the aging phenomena. In this paper, the problem of *SOC* and *SOH* monitoring by the battery management system (BMS) is addressed. In the first part of this work, the *SOC* estimation problem is discussed in detail. In the second part, an estimation algorithm for capacity monitoring is proposed and estimation results are shown. A general approach to monitor the battery *SOH* combined with the *SOC* estimation is also discussed.

The easiest way to estimate the actual *SOC* is by evaluating the ratio between the amount between the energy stored in the battery and the battery capacity. The main drawback of this approach, though, is that the numerical integration done in-vehicle is very sensitive to the *SOC* initial condition, not always accurately known. Moreover, the result of the integration can easily drift or diverge due to the presence of additional noise (Chicago Electric Bicycles LLC, http://www.chicagoelectricbicycles.com).

For, different methods falling in the category of *indirect methods* have been developed in the literature to estimate *SOC* (Pang et al., 2001; Chang, 2013; Coleman et al., 2007; Chiasson and Vairamohan, 2005; Barbarisi et al., 2006; Piller et al., 2001;

Rubagotti et al., 2009; Plett, 2004; Lee et al., 2008; Vasebi et al., 2007; He et al., 2011; Han et al., 2009). For instance, *SOC* can be computed starting from open circuit voltage, V_{OCV}, measurement (Chiasson and Vairamohan, 2005). Both for lead-acid and most Li-ion batteries, the *SOC* estimation with this method is straight-forward due to the linear relationship of the V_{OCV} with respect to the *SOC*. By contrast, when the relationship V_{OCV} (*SOC*) shows a flat region for a large range of *SOC* values, it is harder to translate the V_{OCV} measurement to *SOC* values (Chang, 2013; Coleman et al., 2007).

Indirect methods can also be developed using reduced state-space electrochemical models. Online *SOC* estimation is performed together with the identification of the model parameters using model-based methods for state estimation (Barbarisi et al., 2006; Di Domenico et al., 208). Other methods have been used in literature, such as artificial neural networks and impedance spectroscopy. These methods usually require a large computational effort and very accurate measurements (Piller et al., 2001) which make them suitable for laboratory application only (Chang, 2013).

For on-board vehicle applications, as in the case of e-bike, *SOC* estimation is performed from real-time measurements (voltage and current) using model-based methods. In this paper, two model-based estimation algorithms are developed and compared: extended Kalman filter (EKF) and an adaptive extended Kalman filter (AEKF), using an experimentally validated equivalent circuit-based model (ECM) of the battery (Taborelli and Onori, 2014).

The EKF has been successfully used to estimate the state vector of a nonlinear state-space system model subject to noise. When using EKF, the state estimation is performed based on a comparison between the output obtained from the model and the measured quantities from the plant sensors. The state-space model is defined in such a way the state and the output equations are affected by Gaussian white noises. These noises are defined in terms of mean and covariance and a complete knowledge of these statistical properties is assumed (Fathabadi et al., 2009). The choice of constant values for these parameters has direct effect on the estimation performance and is not always straightforward. It is often the case to treat the noise covariance on the state and the output equation as design parameters. For example, a large covariance on the output means noisy measurements and a 'slow' response of the filter. By contrast, a larger covariance on the state is related to uncertainties on the model and reliable measurements, leading to a 'fast' filter convergence.

In battery applications, examples of *SOC* estimation using EKF are in Rubagotti et al. (2009), Plett (2004), Lee et al. (2008) and Vasebi et al. (2007).

The main drawback of EKF resides in the fact that the correct value of the process covariance matrix is needed. To address this issue, in this paper we pursue the design of the AEKF. In AEKF, the covariance of the process noise is not assumed to be constant, but adaptively updated as new measurements are available.

AEKF has been applied in different research fields, such as robotic applications, track reactor monitoring and internal navigation system/global positioning systems (INS/GPS). An adaptive update of the covariance matrix improves the estimation results as opposed to a fixed choice. For example, in Jetto et al. (1999), an AEKF is implemented to estimate the position of a mobile robot, considering a covariance matrix with a fixed structure, apart from a scaling factor which is adaptively changed, and in Fathabadi et al. (2009), the adaptive filter is used to deal with asynchronous measurement in a tank reactor. The AEKFs have been successfully used to solve the INS/GPS position tracking problem as well (Hide et al., 2003, 2004; Ding et al., 2006; Mohamed and Schwarz, 1999).

The AEKF algorithm has been used for battery *SOC* estimation of a generic Li-ion battery in Charkhgard and Farrokhi (2010) where the process covariance matrix is updated online with a dedicated estimator. In He et al. (2011), an electric vehicle battery is studied and the adaptive algorithm is activated only when the *SOC* estimation is diverging in order to keep it stable. In Han et al. (2009), a solution similar to the one proposed in this paper is developed for a lead-acid battery.

In this work, the problem of designing advanced BMSs is addressed for a Li-ion battery system developed by *AllCell Technologies*.[1] The main purpose is to design a reliable algorithm for an accurate detection of *SOC* and to propose a method to monitor the battery aging. These algorithms are developed for the new categories of light vehicle such as e-bikes. In Section 2, the battery pack structure is discussed and the mathematical model is introduced. In Section 3, the model parameters are identified: for the battery pack resistance identification two methods are discussed and the dependence on *SOC* is discussed. The *SOC* estimation algorithms, i.e., EKF and AEKF are presented in Section 4 along with simulation results obtained from experimental data. In Section 5, the problem of *SOH* estimation is addressed: an algorithm for battery capacity estimation is designed and a generalised framework for combined *SOC*/*SOH* estimation is proposed. Capacity estimation preliminary results obtained from experimental data collected from an aging campaign are shown. Conclusions and future work are outlined in Section 6.

2 Battery modelling

In this section, a description of the battery pack is provided and a mathematical model of the battery is defined.

2.1 Battery pack topology

The battery pack used in the e-bike application studied in this paper is made of 40 LG ICR18650MG1 cells. The cells have a nominal voltage of 3.7 V and a rated capacity of 2.6 Ah. In order to achieve the voltage and capacity requirements, the battery pack has the *10s4p* topology: ten *modules* connected in series, each of them composed by four cells in parallel as shown in Figure 1.

Figure 1 Battery pack topology 10s4p
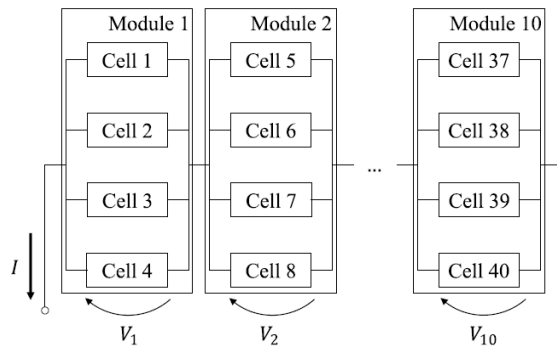
The ten modules in series will provide a total battery pack voltage of $V_{nom} = 37$ V, whereas the pack rated capacity is $Q_{nom} = 10.4$ Ah, being the pack current I the same in each module. In this work, we model the battery pack as an average cell equivalent to a single module, as shown in Figure 2: all battery pack quantities are referred to as average cell quantities.

Figure 2   Battery pack modelled as an average cell: equivalence between the average cell and a single module
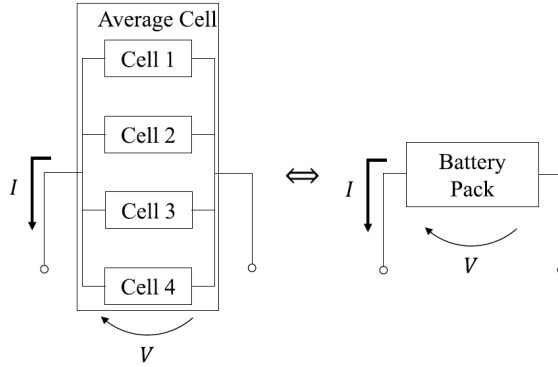
The average cell current is equivalent to the battery pack current I measured by the BMS and a measurement of the voltage across each module, V_i, is available. The average cell voltage, V, is computed by the BMS as the average of the ten voltage measurements across the ten modules:

$$V = \frac{1}{10} \sum_{i=1}^{10} V_i \tag{1}$$

It is possible to calculate the average voltage as in (1) since voltage unbalances were not registered between the modules and voltages V_i are all similar. The rated capacity of the average cell is equivalent to the rated capacity of the battery pack, i.e., $Q_{nom} = 10.4$ Ah.

2.2   Battery model

In order to develop a model-based *SOC* estimator, a mathematical model for the average cell is defined. In literature, two categories of models have been proposed for lithium-ion batteries: electrochemical models (Di Domenico et al., 2008; Gomadam et al., 2002; Gu and Wang, 2000) and ECMs (Rubagotti et al., 2009; Tremblay et al., 2007). The ECMs are the ones mostly used for BMS application and system integration today (Gao et al., 2002), due to the low computational requirement (Ceraolo, 2000). One limitation of this kind of models, though, is the difficulty to trace the battery aging phenomena back to the ECM parameters. This is one of the reasons why electrochemical model are being pursuing. Electrochemical models give a physics-based description of the battery processes which take place inside the battery and ultimately, they allow the battery aging phenomena to be described in detail. At the same time, though, they are computational demanding for BMS use, at least with the present technology. The link between ECM and

electrochemical models is found in Ceraolo (2000), where electrochemical impedance spectroscopy technique is used to define the model electric impedances (Zhang et al., 2004; Moss et al., 2008). The identification of electric parameters of ECM is not always straightforward, as dependence on *SOC*, temperature and current amplitude is often included.

In this study, a second order ECM is considered to model the average cell, as shown in Figure 3.

Figure 3   Equivalent circuit representation of the average cell model
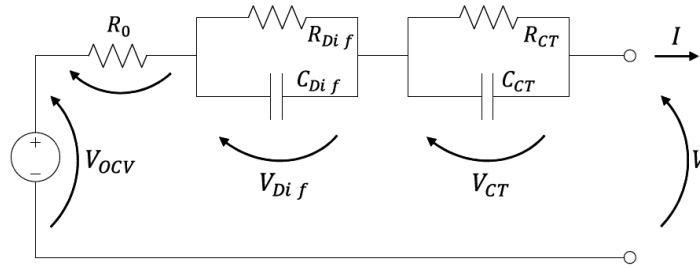
The state space formulation in discrete time domain is:

$$
\begin{cases}
SOC(k+1) = SOC(k) - \dfrac{\Delta t}{Q_{nom}} I(k) \\[2mm]
V_{CT}(k+1) = e^{-\frac{\Delta t}{\tau CT}} V_{Ct}(k) + R_{CT}\left(1 - e^{-\frac{\Delta t}{\tau CT}}\right) I(k) \\[2mm]
V_{Dif}(k+1) = e^{-\frac{\Delta t}{\tau_{Dif}}} V_{Dif}(k) + R_{Dif}\left(1 - e^{-\frac{\delta t}{\tau_{Dif}}}\right) I(k)
\end{cases}
\tag{2}
$$

where *k* is the discrete time instant.

The first equation represents the *SOC* dynamics, in which Δt is the discrete time step. The input current *I(k)* is considered positive during discharging and negative during charging. The two *RC* branches (R_{CT}, C_{CT} and R_{Dif}, C_{Dif}) are used to model the dynamic response of the battery average cell and $\tau_{CT} = R_{CT}C_{CT}$ and $\tau_{Dif} = R_{Dif}C_{Dif}$ are the respective time constants. The parallel branches represent the charge transfer (*CT*) and diffusion (*Dif*) phenomena inside the battery. In Moss et al. (2008), a detailed representation of these phenomena is addressed: diffusion and CT properties are described with more impedance elements and with specific dependence on the input current.

The output equation relates the average output voltage *V(k)* to the voltage drop across the equivalent circuit elements, as follows:

$$
V(k) = V_{OCV}\left(SOC(k)\right) - V_{CT}(k) - V_{Dif}(k) - R_0 I(k)
\tag{3}
$$

where $V_{OCV}(SOC)$ is the average cell open circuit voltage function of *SOC* and R_0 is the battery cell internal resistance.

Defining the state vector as $x(k) = [SOC(k)\ \ V_{CT}(k)\ \ V_{Dif}(k)]^T$, the model input $u(k) = I(k)$ and output $y(k) = V(k)$, the discrete-time nonlinear state space model of the battery can be written as:

$$\begin{cases} x(k+1) = Ax(k) + Bu(k) \\ y(k) = g\big(x(k), u(k)\big) \end{cases} \tag{4}$$

The nonlinearity of the model is in the output equation (3), in that the open circuit voltage is not linear with respect to the state $x(k)$. The state equation, on the other hand, is linear with system matrices defined as:

$$A = \begin{bmatrix} 1 & 0 & 0 \\ 0 & e^{-\frac{\Delta t}{\tau_{CT}}} & 0 \\ 0 & 0 & e^{-\frac{\Delta t}{\tau_{Dif}}} \end{bmatrix}; \quad B = \begin{bmatrix} -\dfrac{\Delta t}{Q_{nom}} \\ RCT\left(1 - e^{-\frac{\Delta t}{\tau_{CT}}}\right) \\ R_{Dif}\left(1 - e^{-\frac{\Delta t}{\tau_{Dif}}}\right) \end{bmatrix} \tag{5}$$

The battery cell model (4) is defined as a function of: the dynamic parameters R_{CT}, C_{CT}; R_{Dif}, C_{Dif}, the open circuit voltage V_{OCV} and the resistance R_0. The identification of these parameters is discussed in the following section.

3   Parameter identification

All the experimental tests, both at cell and pack level, were performed at *AllCell Technologies* and were conducted at ambient temperature.

The tests are described using the C-rate, which is the rate of charge or discharge current in normalised form:

$$C\text{-}rate = \frac{I(k)}{Q_{nom}}[1/h]$$

The general expression C/xx indicates that the number of hours to completely discharge the battery at a constant current is xx.[2]

3.1   Open circuit voltage

The relationship between V_{OCV} and $_{SOC}$ has been identified by subjecting the battery to a constant current discharge of $C/20$ from a fully charged battery.[3] Due to the very small current used to discharge the battery the voltage drop on the internal impedance can be considered negligible so that the measured voltage can be approximated to V_{OCV}.

Figure 4   Open circuit voltage: identified V_{OCV} function of *SOC* (see online version for colours)
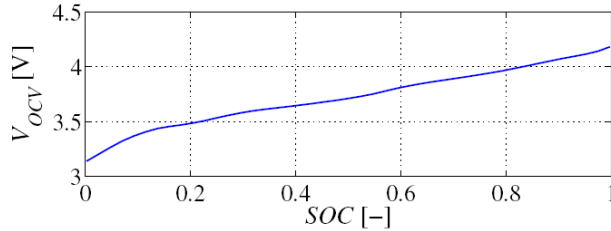
The $V_{OCV}(SOC)$ characteristic is shown in Figure 4, where the *SOC* is evaluated through *Coulomb counting*.

3.2   Dynamic parameters

In order to identify the dynamic parameters R_{CT}, C_{CT}, R_{Dif} and C_{Dif}, an identification test has been performed on the battery cell at the beginning of life (BOL). The *parameter identification test* consists in a series of symmetrical discharge-charge current pulses performed at different *SOC* (Lam et al., 2011; Lin et al., 2014). The test current profile is shown in Figure 5(a) and the corresponding battery voltage response is shown in Figure 5(b). A zoomed current pulse is shown in Figure 5(c) performed at *SOC* = 50% and the corresponding voltage zoom is in Figure 5(d).

The current pulses have a duration of 10 s each, with an amplitude of ± 1*C*. Between two consecutive pulses, a *C*/40 constant current is used to discharge the battery until to the following *SOC* level. The identification procedure applied to identify the dynamic parameters has shown that the dependence of these on *SOC* is negligible, although the wide *SOC* range swept.

The least squares (LSs) method was used for the identification, where the value of the parameters are identified minimising the sum *S* of the squared difference between the experimental measured voltage $V_{exp}^P(k)$ in Figure 5(b), and the voltage predicted by the model (4):

$$\min(S) = \min\left(\sum_{j=T_0}^{T_f} \left[V_{exp}^P(j) - g\left(x(j), u(j)\right) \right]^2 \right) \tag{6}$$

where T_0 and T_f are the initial and final time instants of the experimental test. In (6), the model input $u(j)$ corresponds to the measured current in Figure 5(a), while the state $x(j)$ is evaluated integrating the model (2) starting from the test initial condition: *SOC*(0) = 50%, $V_{CT}(0) = V_{Dif}(0) = 0$ *V*.

The identified parameters values are reported in Table 1.

Table 1   Dynamic parameters values

R_{CT}	1.6 mW
$t_{CT} = R_{CT}C_{CT}$	3.68 s
R_{Dif}	7.7 mW
$t_{Dif} = R_{Dif}C_{Dif}$	84.34 s

3.3   Resistance

To obtain the model resistance, two methods were investigated:

1   real-time estimation through an EKF

2   identification with LS method.

Both methods are described and compared in the following. A dedicated identification test, referred to as R_0-*identification test*, was designed and performed at pack-level at BOL for the sole purpose of identifying the resistance.

Figure 5   Dynamic parameters identification test, (a) battery current $I_{exp}^{P}(k)$ (b) measured voltage $V_{exp}^{P}(k)$ (c) Zoom of battery current $I_{exp}^{P}(k)$ around a pulse performed at *SOC* = 50% (d) Zoom of the measured voltage at *SOC* = 50% (see online version for colours)

Parameter identification test

(a)

(b)

Parameter identification test – zoom
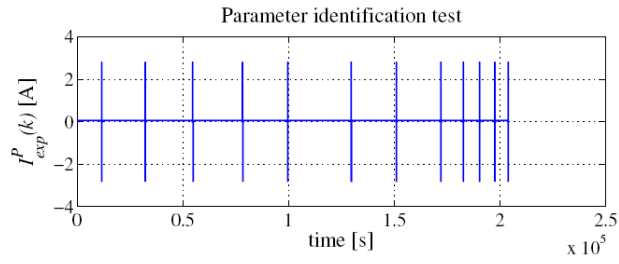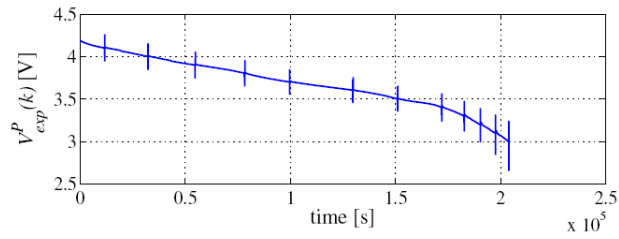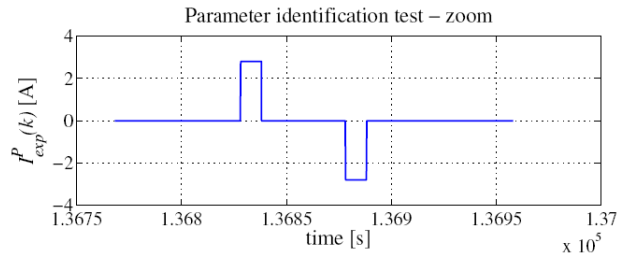
(c)
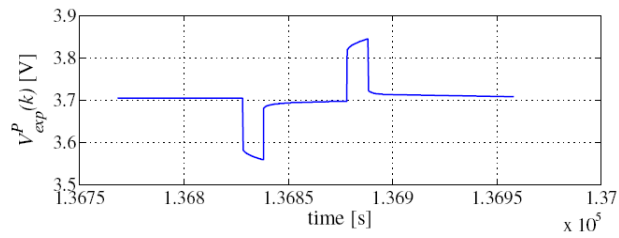
(d)

3.3.1 Extended Kalman filter

In this subsection, EKF is used to estimate the model resistance R_0. Although, the EKF is a well-known algorithm largely used (Welch and Bishop, 1995; Plett, 2004a, 2004b) to estimate the state of a dynamic system characterised by noisy measurements, it can also be used to perform real-time system parameter identification (Plett, 2004b).

The discharge test current profile $I_{exp}^R(k)$ is shown in Figure 6(a) and the average cell voltage response $V_{exp}^R(k)$ is in Figure 6(b). During the test, the battery is completely discharged, starting from a fully charged condition.

Figure 6 R_0-*identification test*, (a) average cell current $I_{exp}^R(k)$ (b) measured average cell voltage, called $V_{exp}^R(k)$ (see online version for colours)

(a)

(b)
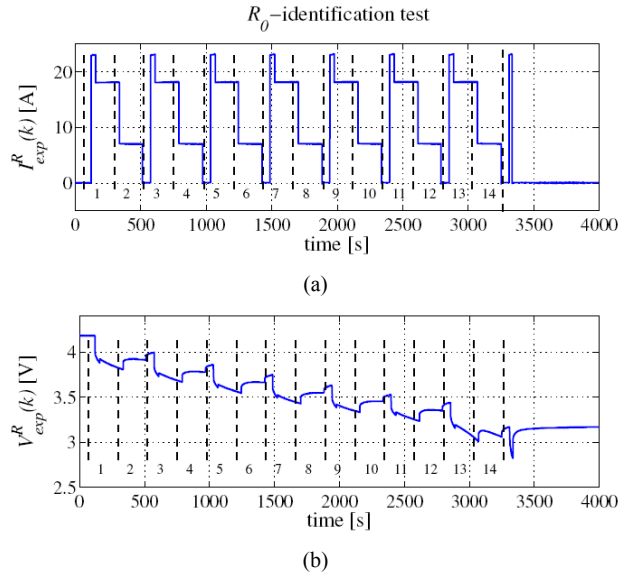
With reference to the e-bike application, only discharge scenario is evaluated, since regeneration is not possible for this application.

In addition to the resistance identification, the EKF is used to identify the battery capacity Q_{nom} at BOL.[4]

Following the same structure proposed in Plett (2004b), the parameters to identify are included in the parameter vector θ:

$$\theta = \begin{bmatrix} R_0 & Q_{nom} \end{bmatrix}^T \tag{7}$$

Hence, the state space battery model (4) can be written as:

$$\begin{cases} x(k+1, \theta) = Ax(k) + B(\theta)u(k) \\ y(k, \theta) = g\big(z(k), u(k), \theta\big) \end{cases} \tag{8}$$

where the dependence of the model equations on the parameters vector θ is now made explicit.

The EKF is a model-based method for state estimation. To identify the vector of parameters, θ has to be made as state of a proper state space model. For this reason, θ is modelled as:

$$\theta(k+1) = \theta(k) + v_\theta(k) \tag{9}$$

where $v_\theta \sim \mathcal{N}(0, Q_\theta)$ is a Guassian white noise, with zero mean and covariance Q_θ. Model (9) is justified by the fact that the aging parameters R_0 and Q_{nom} vary slowly compared to the system dynamics (4) thus to be assumed constant over the duration of R_0-identification test. The noise v_θ models the uncertainties associated with the model (9). Given that the constant dynamic behaviour of θ is accurate, the covariance of v_θ is set to be small.

The output equation is a function of the system parameters θ:

$$y_\theta(k, \theta) = g\big(x(k), u(k), \theta(k)\big) + w_\theta(k) \tag{10}$$

where $w_\theta \sim \mathcal{N}(0, R_\theta)$ is a Gaussian white noise with zero mean and covariance R_θ, which represents the model output noise.

The EKF is based on the implementation of prediction step and correction step (Rubagotti et al., 2009); a summary of EKF algorithm equations is shown in Table 2.

Table 2   EKF algorithm for parameters identification: prediction step and correction step

---

Prediction step:

$$\hat{\theta}^-(k) = \hat{\theta}(k-1) \tag{11a}$$

$$P_\theta^-(k) = P_\theta(k-1) + Q_\theta \tag{11b}$$

Correction step:

$$L_\theta(k) = P_\theta^-(k)C_\theta(k)^T\left(C_\theta(k)P_\theta^-(k)C_\theta(k)^T + R_\theta\right)^{-1} \tag{12a}$$

$$\hat{\theta}(k) = \hat{\theta}^-(k) + L_\theta(k)\left[V_{exp}^R(k) - g\big(x(k), u(k), \hat{\theta}^-(k)\big)\right] \tag{12b}$$

$$P_\theta(k) = \big(I - L_\theta(k)C_\theta(k)\big)P_\theta^-(k) \tag{12c}$$

The estimated parameters vector is $\hat{\theta}$ and P_θ is the covariance matrix of the estimation error defined as: $e_\theta(k) = \theta - \hat{\theta}$. In the prediction step, the estimated state $\hat{\theta}$ and matrix P_θ are projected to the next time step using the model equation in (9), and the noise covariance Q_θ. The superscript minus indicates that these quantities in (11a) and (11b) have not yet been corrected using the measurements (Rubagotti et al., 2009). In the correction step, the parameter vector estimation $\hat{\theta}$ and the covariance P_θ are corrected by using the information from the measurements V_{exp}^R and the adapted Kalman gain L_θ. In this way, $\hat{\theta}$ is the parameters vector estimated in order to reduce the difference between the experimental voltage $V_{exp}^R(k)$ and the model response $g(x(k), u(k), \hat{\theta}^-(k))$. It has to be noted that the model state $x(k)$ is needed to evaluate this last term: it is computed integrating the system equations (2) using the dynamic parameters identified in

Subsection 3.2, starting from the initial conditions of the R_0-*identification test*, namely $SOC(0) = 100\%$, $V_{CT}(0) = V_{Dif}(0) = 0$ V.

The matrix C_θ, used in (12a) and (12c), is the linearisation of the nonlinear output equation (10), with respect to the vector of parameters θ:

$$C_\theta(k) = \frac{dg\left(x(k), u(k), \theta(k)\right)}{d\theta}\bigg|_{\theta=\hat{\theta}^-(k)} \tag{13}$$

As also shown in Plett (2004b), since $g(x(k), u(k), \theta(k))$ is a nonlinear function of both the parameters vector $\theta(k)$ and the model state $x(k)$, (13) can be written as:

$$\frac{dg(x, u, \theta)}{d\theta}\bigg|_k = \frac{\partial g(x, u, \theta)}{\partial \theta}\bigg|_k + \frac{\partial g(x, u, \theta)}{\partial x}\bigg|_k \left(\frac{dx}{d\theta}\bigg|_k\right) \tag{14}$$

$$\frac{dx}{d\theta}\bigg|_k = \frac{dB(\theta)}{\partial \theta}\bigg|_{k-1} u(k-1) + A\left(\frac{dx}{d\theta}\bigg|_{k-1}\right) \tag{15}$$

The term $\frac{dx}{d\theta}$ is initialised at 0 and evolves following the dynamics in (15). In this work, since the vector θ is defined as in (7), through (14) and (15) the matrix $C_\theta(k)$ can be computed as:

$$C_\theta(k) = \begin{bmatrix} I(k) & 0 \end{bmatrix} + C(k)\left[\begin{bmatrix} 0 & \dfrac{\Delta t I(k-1)}{Q_{nom}^2(k-1)} \\ 0 & 0 \\ 0 & 0 \end{bmatrix} + A\dfrac{dx(k-1)}{d\theta}\right] \tag{16}$$

where $C = \frac{\partial g(x, i, \theta)}{\partial x}$ and A is the dynamic matrix of the battery model in (5).

The values used for the state and output noise covariances are $Q_\theta = \begin{bmatrix} 10^{-6} & 0 \\ 0 & 10^{-4} \end{bmatrix}$ and $R_\theta = 10$. The noise v_θ has a weak effect on the constant dynamics of the parameters, while a larger output covariance is accepted for w_θ, in order to consider generic uncertainties on the overall battery model.

In Figure 7, the estimated resistance $\hat{R}_0$ is shown as a function of time (dashed line). In Figure 8, it is shown a comparison between the experimental voltage $V_{exp}^R(k)$ and the output voltage $\hat{V}_{mod}(k)$ obtained from the average cell model when the estimated resistance $\hat{R}_0$ is used and the test current I_{exp}^R in Figure 6(a) is given as an input. To quantify how close the model output is to the measurements, the voltage error $\tilde{e}_{EKF}$ is evaluated as:

$$\tilde{e}_{EKF}(k) = V_{exp}^R(k) - \hat{V}_{mod}(k) \tag{17}$$

The error $\tilde{e}_{EKF}$ is shown in Figure 9 and its RMS value[5] is shown in Table 3.

Figure 7   Resistance R_0: comparison between $\hat{R}_0$ estimated with EKF and $\tilde{R}_0$ identified with LS
approach, function of time (see online version for colours)
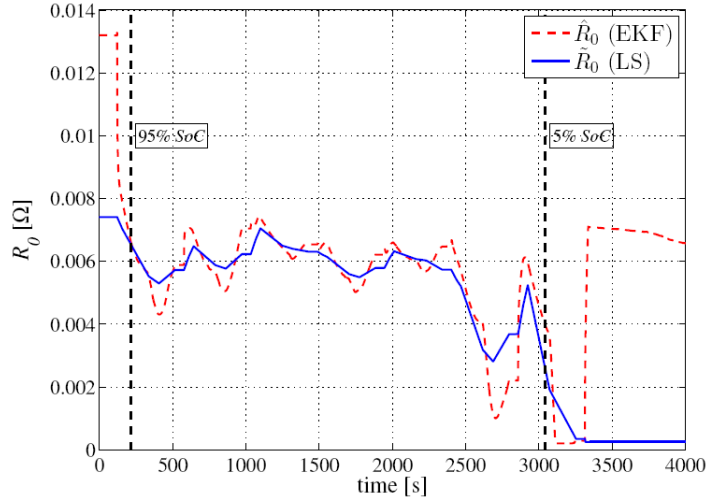
Figure 8   Comparison between average cell experimental voltage $V_{\exp}^R(k)$, model output voltage
$\hat{V}_{\mathrm{mod}}(k)$ evaluated with $\hat{R}_0(EKF)$ and $\tilde{V}_{\mathrm{mod}}(k)$ evaluated with $\tilde{R}_0(LS)$ (see online
version for colours)
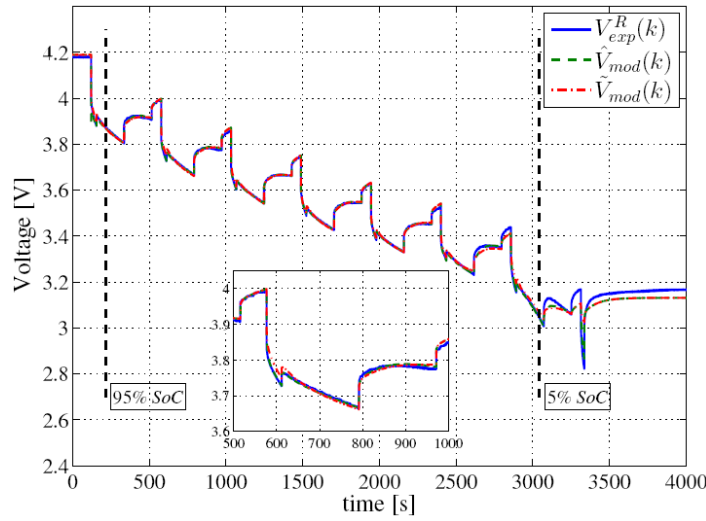
The capacity value $\hat{Q}_{nom}$ estimated with this approach is practically constant over the
simulation time window, and equivalent to the nominal value Q_{nom} = 10.4 Ah, which
confirms the nominal capacity value at BOL used in the battery model.

In Figure 7, dependence of $\hat{R}_0$ on *SOC* is noticeable.

Figure 9   Comparison between the voltage error $\tilde{e}_{EKF}(k)$ and $\tilde{e}_{LS}(k)$ (see online version for colours)
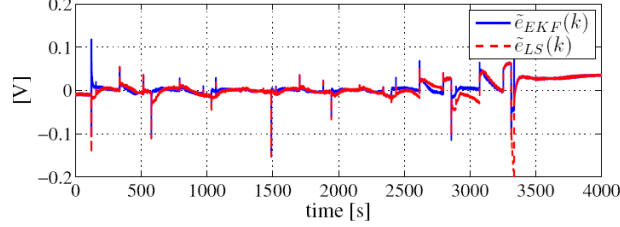
3.4   *LSs method*

In this subsection, a LS method is implemented to identify the resistance dependence $R_0(SOC)$ on the *SOC*.

The input and output data from R_0-*identification test* are divided into *SOC* batches, as shown in Figure 6 (vertical dashed lines). The identification procedure is the same as discussed in Subsection 3.2, but in this case the LS algorithm is applied on a single batch *i*. For each batch *i*, a constant resistance value $\tilde{R}_{0,i}$ is identified minimising the sum of the squared difference S_i between the experimental measured voltages $V_{exp,i}^R$ and the voltage predicted by the model output from (4):

$$\min\left(S_i\right) = \min\left(\sum_{j=T_{0,i}}^{T_{f,i}} \left(V_{exp,i}^R(j) - g\left(x(j), u(j), \tilde{R}_{0,i}\right) \right)^2 \right) \tag{18}$$

where $T_{0,i}$ and $T_{f,i}$ are the initial and final time instants of each batch *i* respectively. As shown in Section 2, the output function $g(\cdot)$ has a linear dependence on the parameter $\tilde{R}_{0,i}$ and the input $u(k)$, and it is nonlinear with reference to the model state $x(k)$. To apply the LS method, the input $u(k)$ and the state $x(k)$ are known at each time instant, the former from experimental data $I_{exp}^R(k)$ [Figure 6(a)] and the latter from the model, computed integrating equation (2).

For each batch *i*, the average *SOC*, SOC_i, is calculated, to relate the identified resistance values $\tilde{R}_{0,i}$ to the corresponding SOC_i. The identified resistance $\tilde{R}_0(SOC)$ is shown in Figure 10 function of *SOC*. Since $SOC(k)$ is a known function of time from the model equation, in Figure 7 (solid line) $\tilde{R}_0$ is shown as a function of time. Comparing $\hat{R}_0$ evaluated with EKF and $\tilde{R}_0$ with LS method both as a function of time, from Figure 7, it can be seen that the two show similar trends over the entire *SOC* range except for high *SOC* (beginning of discharging, 99% *SOC*) and low *SOC* values (1% *SOC*).

Also in the case of LS, the voltage error $\tilde{e}_{LS}$ is evaluated as the difference between experimental voltage $V_{exp}^R(k)$ and the model output $\tilde{V}_{mod}$:

$$\tilde{e}_{LS}(k) = V_{\exp}^R(k) - \tilde{V}_{\mod}(k) \tag{19}$$

The voltage $\tilde{V}_{\mod}$ is obtained as the output of the average cell model, when $\tilde{R}_0(SOC)$ is used. $\tilde{V}_{\mod}(k)$ is compared to the experimental voltage $V_{\exp}^R(k)$ and to the model output voltage $\hat{V}_{\mod}(k)$ (using EKF to estimate the resistance) in Figure 8. The error $\tilde{e}_{LS}$ is shown in Figure 9.

In Table 3, the RMS value of $\tilde{e}_{EKF}$ and $\tilde{e}_{LS}$ are compared.

Table 3   Validation RMS error, comparison between EKF method and LS approach

Error	RMS value
$\tilde{e}_{EKF}(k)$	0.01702 V^2
$\tilde{e}_{LS}(k)$	0.02160 V^2

Figure 10   Resistance $\tilde{R}_0(SOC)$ function of *SOC* (see online version for colours)
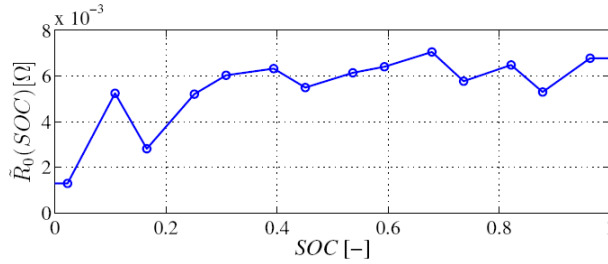
Although the two estimation methods studied in this section provide very close performance, as also shown by the RMS values of $\tilde{e}_{EKF}$ and $\tilde{e}_{LS}$ in Table 3, the resistance identified with EKF (see, Figure 7 shows meaningful values in a *SOC* range from 95% to 5%. Outside of this *SOC* range the unmodelled dynamics affects the EKF estimation performances. For these reasons, in this work we chose to use the resistance identified with the LS method $\tilde{R}_0(SOC)$.

Model validation

In order to validate the model, a validation test designed performed on the battery pack at BOL. This test represents a generic usage scenario for the battery, related to the light electric-vehicle application.

The *validation test* is a discharge test, through $I_{\exp}^V(k)$, performed from a fully charged condition [see, Figure 11(a)]. It is made by a series of steps at three different levels of C-rate, up to a maximum current value of 2*C*. The average cell output voltage $V_{\exp}^V(k)$ measured by the BMS is shown in Figure 11(b).

The model validation results are shown in Figure 11(b), where the experimental voltage $V_{\exp}^V(k)$ is compared with the model output voltage $V_{\mathrm{mod}}(k)$ evaluated with (3) using the values of the parameters identified previously. The mismatch between the modelled and the measured voltage after the voltage relaxed beyond 4,000s [Figure 11(b)] is due to the fact that model is experimentally calibrated and accurate over a predefined range of *SOC*, and beyond that point, its predictability is lost.

The validation error $e^V(k)$ given by the difference between the experimental voltage $V_{\exp}^V(k)$ and the model output voltage $V_{\mathrm{mod}}(k)$ is:

$$e^V(k) = V_{\exp}^V(k) - V_{\mathrm{mod}}(k) \tag{20}$$

with an RMS value for $e^V(k)$ of 0.0419 V^2.

Figure 11 Validation test, (a) average cell current; (b) comparison between measured average cell voltage, called $V_{\exp}^V(k),$ and the average cell model output voltage $V(k)$ (see online version for colours)

(a)

(b)
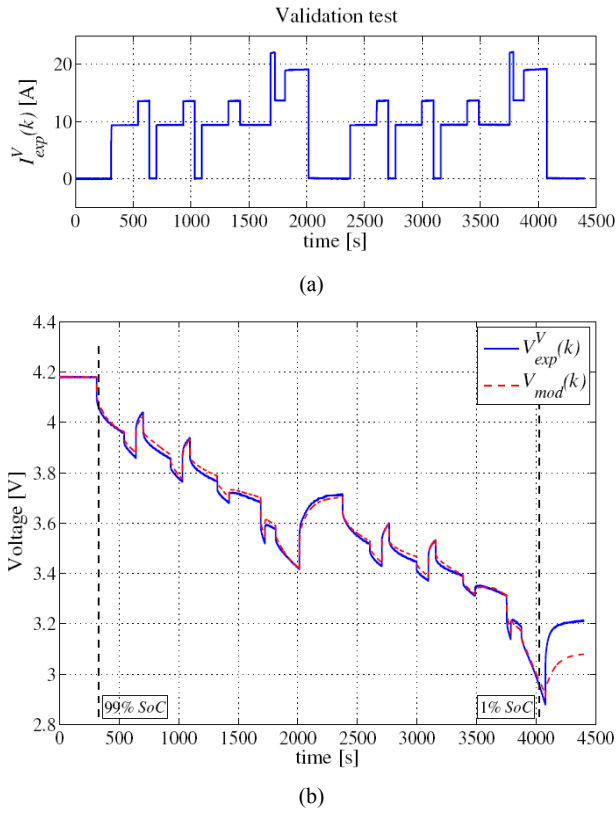
4   SOC estimation algorithms

The *SOC* estimation problem for an e-bike application is addressed in this section, with the purpose to define an algorithm suitable for on board implementation to improve the battery usage and the vehicle power management. Two algorithms are proposed for the *SOC* estimation: EKF and AEKF.

4.1   Extended Kalman filter

The EKF method is proposed to estimate the *SOC* of the battery system described by the nonlinear model (4). When including the process and measurement Gaussian noises, model (4) assumes the general form:

$$\begin{cases} x(k+1) = Ax(k) + Bu(k) + v(k) \\ V(k) = g\left(x(k), u(k)\right) + w(k) \end{cases} \tag{21}$$

where $v(k) \sim \mathcal{N}(0, Q)$ and $w(k) \sim \mathcal{N}(0, R)$ are Gaussian white noises with zero mean and covariance matrix Q for the model state equation and R for the output relation, respectively. A description of the Kalman prediction and correction steps was given in Section 3.3. The estimator equations are summarised in Table 4.

The quantity $\hat{x}(k)$ is the estimated state, and $L(k)$ and $P = E[e(k) \cdot e(k)^T]$ are the Kalman gain and the covariance matrix of the estimation error, defined as: $e(k) = x(k) - \hat{x}(k)$.

The matrix $C(k) = \left.\frac{\partial g(x, I)}{\partial x}\right|_{\hat{x}^-(k), u(k)}$, used in the filter equations (23a) and (23c), is the linearised output matrix $g(x, u)$ around the point $(\hat{x}^-(k), u(k))$, and $V_{\exp}(k)$ in equation (23b) is the actual voltage measured by the BMS.

The covariance matrix Q of the process noise is designed under the assumption that there is no correlation between the noise on the cross state components (Vasebi eta l., 2007), leading to a diagonal structure. The state noise $v(k)$ represents the model uncertainties as well as the approximation due to the neglected nonlinearities (Lee et al., 2008).

Table 4   Summary of EKF algorithm equations

Prediction step:

$$\hat{x}^-(k) = A\hat{x}(k-1) + Bu(k-1) \tag{22a}$$

$$P^-(k) = AP(k-1)A^T + Q \tag{22b}$$

Correction step:

$$L(k) = P^-(k)C(k)^T \left(C(k)P^-(k)C(k)^T + R\right)^{-1} \tag{23a}$$

$$\hat{x}(k) = \hat{x}^-(k) + L(k)\left[V_{\exp}(k) - g\left(\hat{x}^-(k), u(k)\right)\right] \tag{23b}$$

$$P(k) = \left(I - L(k)C(k)\right)P^-(k) \tag{23c}$$

The proposed matrix $Q = \begin{bmatrix} 1,000 \cdot R & 0 & 0 \\ 0 & 0.1 \cdot R & 0 \\ 0 & 0 & 0.01 \cdot R \end{bmatrix}$, defined with reference to the

matrix R, has a higher weight on the first component of the state vector, i.e., the *SOC*.

The output noise covariance R is evaluated using the experimental data and considering the model voltage error $\tilde{e}_{LS}(k)$ computed with (19): from a statistical analysis of the error itself, it can be shown that $\tilde{e}_{LS}(k)$ is well-approximated by a Gaussian distribution with zero mean and the covariance value $R = 4.666 - 10^{-4}$.

In the next subsection an adaptive version of the EKF is presented.

4.2   Adaptive extended Kalman filter

The AEKF proposed in this work is based on the work developed in Mohamed and Schwarz (1999) for INS/GPS application. An adaptive update of matrix Q can help in overcoming the uncertainties in the state noise representing model uncertainties due to the identification process and nonlinearities not modelled.

Usually, the estimation performances of the adaptive solution are evaluated through the information represented by the innovation sequence $d(k)$. The innovation $d(k)$ is defined as:

$$d(k) = V_{\exp}(k) - g\left(\hat{x}^-(k), u(k)\right) \tag{24}$$

which is the difference between the experimental voltage $V_{\exp}(k)$ measured by the BMS and the predicted value $g(\hat{x}^-(k), u(k))$. In $d(k)$ the predicted voltage is computed by the model output equation when the state in the prediction step $\hat{x}^-(k)$ is taken into account.

The innovation covariance matrix is computed as:

$$\hat{D}(k) = \frac{1}{N}\sum_{i=i_0}^{N} d(i)d(i)^T \tag{25}$$

using a moving average of the innovation $d(k)$ in (24), within a moving estimation window of size N, where $i_0 = k - N + 1$ is the first instant of the window.

Matrix $\hat{D}(k)$ represents the actual performance of the estimation process, so that it is a crucial element to be used in defining the adaptive law for matrix Q. The choice of the window length N becomes a design parameter for the algorithm: it must be not so small to correctly represent the estimation performances and at the same time, for on-board implementation, it has to consider the memory available on a physical board.

Starting from the evaluation of $\hat{D}(k)$, the *innovation-based adaptive Kalman filter* can be used, as demonstrated in Mohamed and Schwarz (1999)]. The innovative contribution in Mohamed and Schwarz (1999) is the formulation of the filter in terms of maximum likelihood (ML) estimator. The advantage of this approach is to define the traditional EKF estimator function of some adaptive parameters, usually the process and measure noise covariances Q and R. A ML equation is also defined, as function of the same adaptive parameters. In this work, the only adaptive parameter considered is the process noise covariance matrix Q. The ML equation represents the mathematical

condition which allows to derive an adaptive law for the matrix Q function of the innovation covariance matrix $\hat{D}(k)$. Under the assumption that the measurement noise covariance R is taken as constant, the ML equation in Mohamed and Schwarz (1999) can be transformed in:

$$\hat{Q}(k) = \frac{1}{N}\sum_{i=i_0}^{N}\Delta\hat{x}(i)\Delta\hat{x}(i)^T + P(k) - AP(k-1)A^T \tag{26}$$

where $\Delta\hat{x}$ is the state correction:

$$\Delta\hat{x}(k) = \hat{x}(k) - \hat{x}^-(k) \tag{27}$$

evaluated as the difference between the state before and after updates. From (23b):

$$\Delta\hat{x}(k) = L(k)d(k) \tag{28}$$

Substituting (28) into (26), $\hat{Q}(k)$ can be computed as (Mohamed and Schwarz, 1999):

$$\hat{Q}(k) = L(k)\hat{D}(k)L(k)^T \tag{29}$$

Thus, the AEKF algorithm for the *SOC* estimation uses the same equations of the EKF summarised in Table 4, with the difference that equation (22b) is now implemented using $\hat{Q}(k)$ in (29) as:

$$P^-(k+1) = AP(k)A^T + \hat{Q}(k)$$

4.3   *Simulation results*

EKF and AEKF algorithms are tested over two experimental tests: the R_0-*identification test* of Figure 6 and the validation test of Figure 11 where V_{exp}^R and V_{exp}^V are the measured voltages in those cases. We refer to $\hat{SOC}_{EKF}$ and $\hat{SOC}_{AEKF}$ as the estimated *SOC* evaluated with EKF and AEKF algorithms, respectively. A comparison between the estimation results is shown in Figure 12 with reference to the R_0-*identification test* and in Figure 14 for the *validation test*. As a reference for the comparison, *SOC* obtained with Coulomb counting method (SOC_{cc}) is considered, defined by the discrete-time dynamic equations:

$$SOC_{cc}(k+1) = SOC_{cc}(k) - \frac{\Delta t}{Q_{nom}}I(k) \tag{30}$$

In both cases, in order to test the convergence of the filters, the model state was estimated starting from the initialisation state values equal to $x(0) = [0.4\ 0\ 0]^T$, corresponding to an initial $SOC(0) = 0.4$, while the actual *SOC* level is close to 1, since the battery is fully charged in both tests. In Figure 16, a zoom of initial dynamics of $\hat{SOC}_{EKF}$ and $\hat{SOC}_{AEKF}$ is shown, with reference to the R_0-*identification test*. A rapid convergence of both EKF and AEKF to the *SOC* = 1 is shown.

Figure 12 Comparison between *SOC* estimation results with reference to the R_0-*identification test* (Figure 6): reference Coulomb counting $SOC_{cc}(k)$, $S\hat{O}C_{EKF}(k)$ estimated with EKF and $S\hat{O}C_{AEKF}(k)$ estimated with AEKF (see online version for colours)
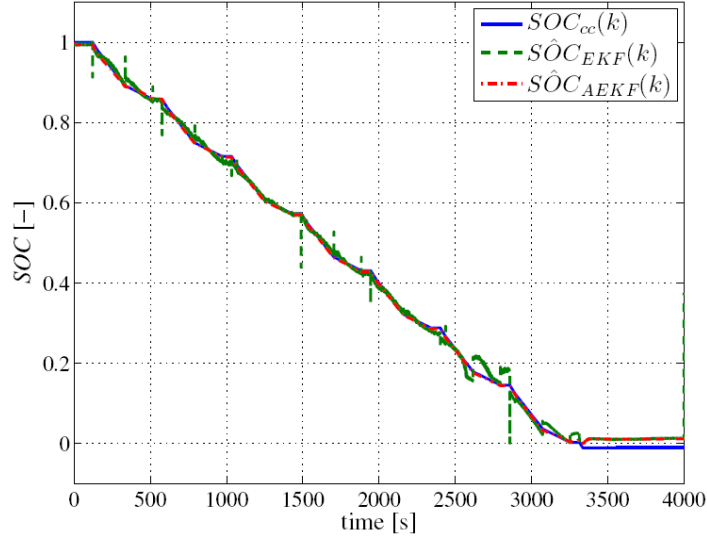
Figure 13 Comparison between *SOC* estimation error $e_{EKF}(k)$ and $e_{AEKF}(k)$ with reference to the R_0-*identification* (Figure 6) (see online version for colours)
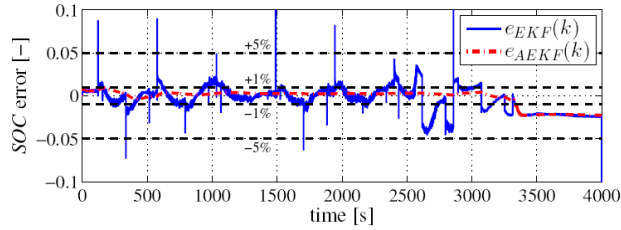
The EKF and AEKF estimation errors are defined as the difference between SOC_{cc} from Coulomb counting and the estimated states of charge $S\hat{O}C_{EKF}$ and $S\hat{O}C_{AEKF}$, respectively:

$$e_{EKF}(k) = SOC_{cc}(k) - S\hat{O}C_{EKF}(k) \tag{31}$$

$$e_{AEKF}(k) = SOC_{cc}(k) - S\hat{O}C_{AEKF}(k) \tag{32}$$

The estimation errors are shown in Figure 13 for the R_0-*identification test* and in Figure 15 for the validation test.

As shown in Figures 13 and 15, using EKF the *SOC* estimation error $e_{EKF}(k)$ is within the 5% range with respect to the SOC_{cc}. This result is tied to the performance of the model in reproducing the battery behaviour: the more accurate the model is, the lower the

estimation error. By contrast, when the model response is less close to the measurements and in particular at low *SOC* values, also the estimation becomes poorer [Figure 8 and Figure 11(b)].

With the AEKF an improvement in the estimation performance is achieved, as shown in Figures 12 and 14. For both tests considered, the estimation error $e_{AEKF}(k)$ remains close to 1% (Figures 13 and 15), which represents an improvement when compared to the EKF, thanks to the adaptive update of the covariace *Q*. In this way, the uncertainty of the model are adaptively compensated since $\hat{Q}(k)$ changes following the estimation error. Also at low *SOC*, the estimation is improved.

As far as the convergence, both filters show a fast response. In AEKF, in particular, the convergence time depends on the initial choice of $\hat{Q}(0)$ in the initialisation phase: the value $\hat{Q}(0) = Q$, corresponding to the constant *Q* used for the EKF, is chosen.

Figure 14   Comparison between *SOC* estimation results with reference to the validation test (Figure 11): reference Coulomb counting $SOC_{cc}(k)$, $S\hat{O}C_{EKF}(k)$ estimated with EKF and $S\hat{O}C_{AEKF}(k)$ estimated with AEKF (see online version for colours)
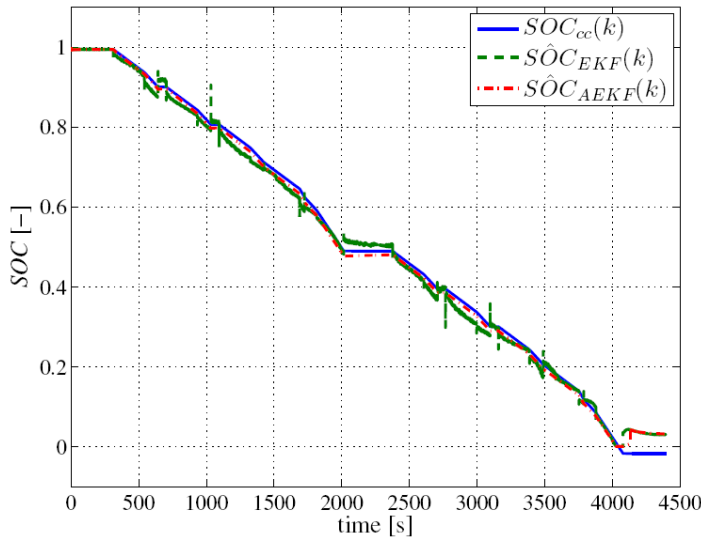
Figure 15   Comparison between *SOC* estimation error $e_{EKF}(k)$ and $e_{AEKF}(k)$ with reference to the validation test (Figure 11) (see online version for colours)
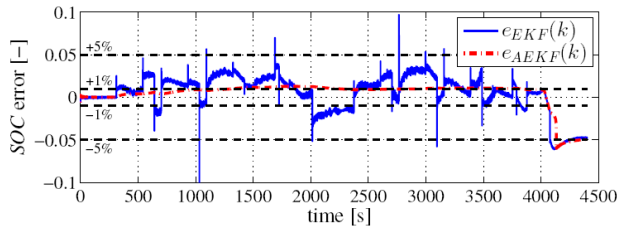
Figure 16   Zoom of the initial dynamics of $\hat{SOC}_{EKF}$ and $\hat{SOC}_{AEKF}$ with reference to the R_0-*identification test* (see online version for colours)
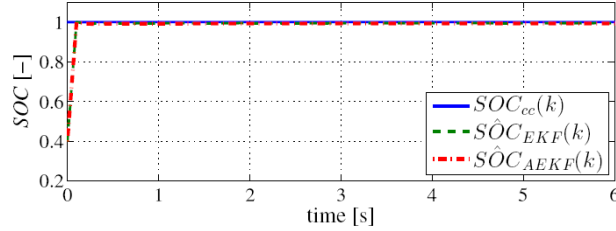
5   Aging parameters estimation

Over the battery lifespan the internal capacity slowly decreases leading to the *capacity fade* phenomenon. The knowledge of the actual value of the battery capacity is an important factor to optimise the battery usage as it allows to accurately estimate the actual residual charge available. In particular, for electric vehicle applications, the problem of capacity estimation is of great interest (Baronti et al., 2013; Kim and Cho, 2011; Remmlinger et al., 2011) as it is directly related to the driving range over vehicle life.

In this section, we present a novel capacity estimation technique hereinafter called *Q-estimation algorithm*. A dual layer estimation structure is provided for a combined *SOC* and *Q* evaluation, according to the structure shown in Figure 17, where the *SOC* estimation is obtained from AEKF. The *Q-estimation algorithm* provides AEKF filter with an update value of the battery capacity, given the actual level of aging. Since the capacity varies very slowly, this value can be estimated and updated with a slower temporal resolution compared with the *SOC* estimator.

Figure 17   Dual layer estimator structure
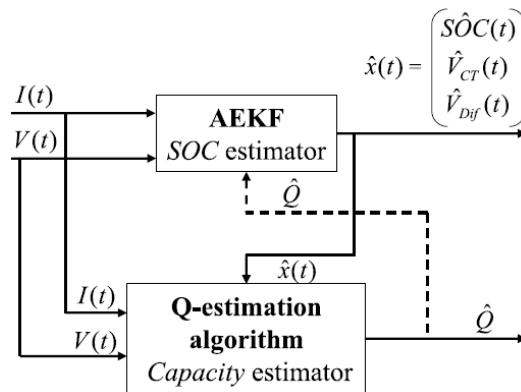
A similar structure of the dual layer algorithm for *SOC* and Q_{batt} estimation is proposed in Rubagotti et al. (2009) and Plett (2004b), with the capacity being estimated by EKF. In these works, a dynamic model of battery capacity is needed to track the evolution of degradation over time. The experimental tests for capacity model identification are lengthy; in addition, the aging behaviour is related to the temperature, *SOC* and C-rate conditions at which the aging tests are performed.

The *Q-estimation algorithm* proposed in this paper provides, on the other hand, an estimation of battery capacity using the measurements collected by the BMS during battery operation. The description of the *Q-estimation algorithm* is carried out using the continuous time version of the state space model of the battery seen in (2), namely

$$
\begin{cases}
\dot{SOC}(t) = -\dfrac{I(t)}{Q_{batt}} \\[2mm]
\dot{V}_{CT}(t) = -\dfrac{1}{R_{CT}C_{CT}}V_{CT}(t) + \dfrac{1}{C_{CT}}I(t) \\[2mm]
\dot{V}_{Dif}(t) = -\dfrac{1}{R_{Dif}C_{Dif}}V_{Dif}(t) + \dfrac{1}{C_{Dif}}I(t)
\end{cases}
\tag{33}
$$

with model output equation:

$$
V(t) = V_{OCV}\big(SOC(t)\big) - V_{CT}(t) - V_{Dif}(t) - R_0\big(SOC(t)\big)\cdot I(t)
\tag{34}
$$

where both V_{OCV} and the internal resistance R_0 are function of *SOC*.

Let us now define the time derivative of the model output voltage $V(t)$:

$$
\dot{V}(t) = \left.\frac{\partial V_{OCV}}{\partial SOC}\right|_{SOC(t)} \cdot \dot{SOC}(t) - \dot{V}_{CT}(t) - \dot{V}_{Dif}(t) - \left.\frac{\partial R_0}{\partial SOC}\right|_{SOC(t)}
$$
$$
\cdot \dot{SOC}(t)I(t) - R_0\big(SOC(t)\big)\dot{I}(t)
\tag{35}
$$

Since $\dot{V}(t)$ is function of the time derivative of all the state components, in (35) we can substitute $\dot{SOC}(t)$, $\dot{V}_{CT}(k)$ and $\dot{V}_{Dif}(t)$ given in (33). Thus, $\dot{V}(t)$ is written as an explicit function of:

• actual capacity value Q_{batt}

• battery current $I(t)$ and its time derivative $\dot{I}(t)$

• voltages across the R*C*-branches, $V_{CT}(t)$ and $V_{Dif}(t)$

• *SOC*, which appears in the term $R_0(SOC)$ and also in $\left.\frac{\partial V_{OCV}}{\partial SOC}\right|_{SOC(t)}$ and $\left.\frac{\partial R_0}{\partial SOC}\right|_{SOC(t)}$. For all of these quantities experimental maps have been identified that can be used once the actual value of *SOC* is known.

The instantaneous values of $SOC(t)$, $V_{CT}(t)$ and $V_{Dif}(t)$ are not physically measurable, but they are estimated from AEKF discussed in Section 4.2. The estimated values are referred to as $\hat{SOC}(t)$, $\hat{V}_{CT}(t)$ and $\hat{V}_{Dif}(t)$.

In addition to the estimated state vector, the battery current $I(t)$ and the measured voltage $V(t)$ are known at each time instant t, along with their time derivative $\dot{I}(t)$ and

$\dot{V}(t)$ which are computed starting from the measurements. Hence, the only unknown parameter in (35) is the capacity value Q_{batt}. In particular $\dot{V}(t)$ results to be a linear function of the unknown parameters Q_{batt}. In order to define a LS estimation problem, equation (35) can be rearranged and written as:

$$W(t) = A(t) \cdot p \tag{36}$$

where

- p is the unknown parameters:

$$p = \frac{1}{Q_{batt}} \tag{37}$$

- $W(t)$ is function of estimated and measured quantities, defined as:

$$
\begin{aligned}
W(t) = \dot{V}(t) - \frac{1}{R_{CT}C_{CT}}\hat{V}_{CT}(t) - \frac{1}{R_{Dif}C_{Dif}}\hat{V}_{Dif}(t) \\
+ \left(\frac{1}{C_{CT}} + \frac{1}{C_{Dif}}\right) I(t) + R_0\left(S\hat{O}C(t)\right)\dot{I}(t)
\end{aligned}
\tag{38}
$$

- $A(t)$ is function of estimated and measured quantities which multiply the unknown parameters in (37):

$$A(t) = -\frac{\partial V_{OCV}}{\partial SOC}\bigg|_{S\hat{O}C(t)} \cdot I(t) \frac{\partial R_0}{\partial SOC}\bigg|_{S\hat{O}C(t)} \cdot I^2(t) \tag{39}$$

Note that the definition of $W(t)$ in (38) (and later in the definition of W_g in (57)) depends on the derivative of the measured output $V(t)$ which might be affected by measurements noise. To attenuate the effect of noise on the measurements differentiators with improved noise suppression can be used (Anderson and Moore, 1979; Benesty and Chen, 2011).

The problem of estimating the unknown parameter p is cast into a linear LS problem, in the form shown in (36). The unknown parameter p is estimated when an excitation signal is given as an input to the system. For this reason, a time window of length n is defined, with n a design parameter. The Q-estimation algorithm consists in the estimation of the unknown capacity over each time window during the battery lifespan. Over the designed time window, $W(t)$ and $A(t)$ are function of estimated or measured quantities as shown in (38) and (39) and $W(t)$ and $A(t)$ are evaluated at each time instant $t_1, t_2, \ldots, t_n$:

$$
[W(t)] = \begin{bmatrix} W(t_1) \\ W(t_2) \\ \ldots \\ W(t_n) \end{bmatrix}; [A(t)] = \begin{bmatrix} A(t_1) \\ A(t_2) \\ \ldots \\ A(t_n) \end{bmatrix};
\tag{40}
$$

where t_1 and t_n are the first and the last time instant inside the designed window, respectively.

The LS problem (36) can be written in the following matrix form:

$$[W(t)] = [A(t)] \cdot p \tag{41}$$

This matrix formulation helps in reducing the numerical errors related to the measurements of $V(t)$ and $I(t)$, to the computations of their time derivatives and to the state estimation performed with AEKF.

From (41), the estimated $\hat{p}$ is obtained to minimise the error function J:

$$\hat{p} = \arg\min J(p) = \left([W(t)] - [A(t)]\,p\right)^T \cdot \left([W(t)] - [A(t)]\,p\right) \tag{42}$$

Writing (42) as:

$$J = [W(t)]^T [W(t)] - [W(t)][A(t)]\,p - p[A(t)]^T [W(t)] + p[A(t)]^T [A(t)]\,p \tag{43}$$

the minimisation is done by calculating:

$$\frac{\partial J}{\partial p} = -2[A(t)]^T [W(t)] + 2[A(t)]^T [A(t)]\,p = 0 \tag{44}$$

From (44), $\hat{p}$ is:

$$\hat{p} = \left([A(t)]^T [A(t)]\right)^{-1} [A(t)]^T [W(t)] \tag{45}$$

The unknown parameter $\hat{p}$ is thus calculated as a matrix product, once the values all the quantities in the matrices $[W(t)]$ and $[A(t)]$ are collected over the designed time window.

5.1   Simulation results

The *Q-estimation algorithm* has been implemented in simulation and tested with experimental data. In this section, simulation results are shown and the implementation details are discussed.

With reference to the e-bike application, during a typical usage condition the battery is discharged starting from a fully charged condition ($SOC = 100\%$) down to lower level of *SOC*.

The *Q-estimation algorithm* is executed over the time window $[t_1\ t_n]$ where:

- t_1 is the time instant when $SOC = 80\%$

- t_n is the time when the *SOC* goes below 40% (*SOC* is estimated with AEKF).

Over the selected *SOC* range, the state estimation performed with AKEF shows the lower estimation error. The matrices $[W(t)]$ and $[A(t)]$ used in the *Q-estimation algorithm* are evaluated over a time window corresponding to the [40% 80%] *SOC*.

The *Q-estimation algorithm* has been applied to the R_0-*identification test* shown in Figure 6 which returns the estimated value of $\hat{Q}_{batt} = 10.3831$ Ah, corresponding to a percentage error of 0.165% from the nominal value $Q_{nom} = 10.4$ Ah.

The *Q-estimation algorithm* is also tested on an aging scenario where the capacity decreases over the battery lifespan. An aging campaign was conducted to age the battery with repetitive charging and discharging cycles. The campaign consists in 500 charging and discharging cycles. The battery is fully charged through the CC-CV protocol at the beginning of each cycle. After the charge phase, a constant current discharge of $1C$,

starting from an open circuit voltage of 4.2 V to a lower value of 3.2 V is applied. The discharge current and the measured voltage for cycle number 1 are shown in Figure 18.

Figure 18   Cycle 1 of the aging campaign, (a) constant current profile of the discharge test (b) measured average cell voltage (see online version for colours)
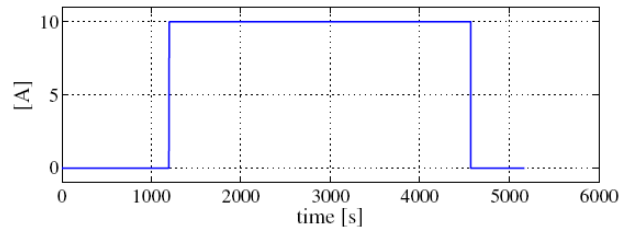
(a)
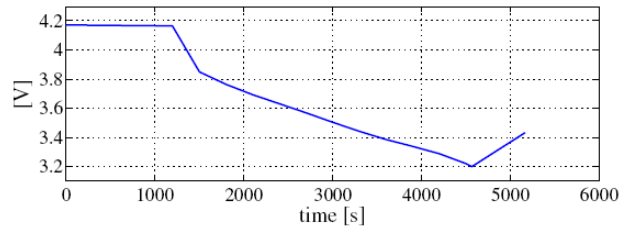
(b)

Figure 19   Capacity estimation results: normalised values with respect to the BOL capacity (see online version for colours)
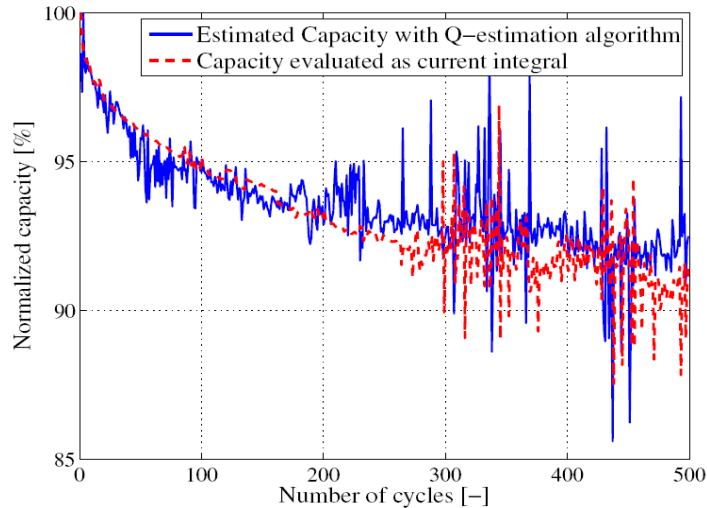
Note: Comparison between the benchmark capacity values evaluated as the current integral and the capacity values estimated with Q-estimation algorithm

It must be outlined that the discharge phase over which the capacity is evaluated, ranging between 4.2 V and 3.2 V, does not constitute a standard capacity test as it does not cover the entire *SOC* range 100%–0%. In fact, over this voltage range, the battery is discharged by an amount of *SOC* equal to ΔSOC_{cycle}. The average ΔSOC_{cycle} value over 500 cycles is 81.84% *SOC*. Since the current integrals are evaluated on the *SOC* range ΔSOC_{cycle} and the cycles are performed with constant current, the benchmark capacity is scaled at each cycle:

$$Q_{current\ integral} = \left(\int_{cycle} I(t)dt \right) \cdot \frac{100}{\Delta SOC_{cycle}} \tag{46}$$

The scaled capacity values have then been used as benchmark to compare the estimation performed by the *Q-estimation algorithm*. In Figure 19, a comparison between the estimated capacity with *Q-estimation algorithm* and the capacity evaluated as current integral using the normalisation (46) is shown.

5.2   *SOC and aging parameters estimation: general approach*

The algorithm introduced in the previous section can be generalised to include both the aging parameters and *SOC* in the estimation. The advantage of this general approach is the estimation of *SOC* obtained at the same time with an update of the model parameters. In this way, a separated algorithm for *SOC* estimation does not need to be implemented as well as a battery aging model is not necessary.

For simplicity, in order to present the general *SOC*/*SOH* estimation framework, we consider the simple case of 1st order ECM, defined in continuous-time as:

$$\begin{cases} \dot{SOC}(t) = -\dfrac{I(t)}{Q_{batt}} \\ \dot{V_1}(t) = -\dfrac{1}{R_1 C_1} V_1(t) + \dfrac{1}{C_1} I(t) \end{cases} \tag{47}$$

where the first equation represents the *SOC* dynamics and the second is the dynamics of the voltage across the parallel of resistance R_1 and capacitance C_1 (we assume one $R_1 C_1$ branch in this case, but extension to the general case of two or more branches is easily performed). The model input is the battery current $I(t)$, positive during discharging and negative during charging, while Q_{batt} is the battery capacity. The battery output voltage is thus defined in continuous-time domain by the equation:

$$V(t) = V_{OCV}(SOC) - V_1(t) - R_{batt} I(t) \tag{48}$$

where V_{OCV} is the open circuit voltage generator in the 1st order ECM, in series with the battery resistance R_{batt} and the parallel of R_1 and C_1.

The generalised estimation algorithm is based on LS method and combines the estimation of *SOC* and the aging parameters, capacity Q_{batt} and resistance R_{batt}, related to capacity fade and power fade phenomena. In particular, the internal resistance R_{batt} is modelled as $R_{batt} = R_0 + \Delta R$, where R_0 is the nominal resistance identified on a battery at BOL and ΔR is the positive resistance increase overtime.

In addition, V_{OCV} is assumed to be a linear function of *SOC* defined as:

$$V_{OCV} = \alpha + \beta \cdot SOC \tag{49}$$

where α and β are constant parameters.

In order to establish a LS estimation problem, the time derivative of equation (48) is computed and given by:

$$\dot{V}(t) = \beta \cdot \dot{SOC}(t) - (R_0 + \Delta R)\dot{I}(t) - \dot{V}_1(t) \tag{50}$$

where the terms $\frac{\partial V_{OCV}}{\partial t} = \beta \frac{\partial SOC}{\partial t}$ and the resistance increment ΔR is treated as a constant over the estimation time window. As done in the previous section, the estimation is performed on a time window of duration n. ΔR and Q_{batt} are slow time-varying parameters since aging phenomena evolve on a different time scale with respect to electrical and *SOC* dynamics.

Substituting the dynamic equation of $\dot{SOC}(t)$ and $\dot{V}_1(t)$ defined in (47) into (50):

$$\dot{V}(t) = -\beta \frac{I(t)}{Q_{batt}} - R_0 \cdot I(t) - \Delta R \cdot \dot{I}(t) + \frac{1}{R_1 C_1} V_1(t) - \frac{1}{C_1} I(t) \tag{51}$$

where $\dot{V}(t)$ is written as explicit function of current $I(t)$ and its derivative and voltage $V_1(t)$.

Voltage $V_1(t)$ is computed from (48) as:

$$V_1(t) = \alpha + \beta \cdot SOC(t) - R_0 \cdot I(t) - \Delta R \cdot I(t) - V(t) \tag{52}$$

where V_{OCV} and the resistance R_{batt} definitions are substituted. Integrating the *SOC* model equation we can write:

$$SOC(t) = SOC(0) - \frac{1}{Q_{batt}} \int_T I(\tau)d\tau \tag{53}$$

where $SOC(0)$ is the initial *SOC* value corresponding to the initial condition when the estimation is performed, and the form $\int_T d\tau$ means that the integral of the battery current is computed over the estimation time window.

Substituting (53) into (52) we obtain:

$$\begin{aligned} V_1(t) = \alpha + \beta \cdot SOC(0) + \\ -\beta \frac{1}{Q_{batt}} \int_T I(\tau)d\tau - R_0 \cdot I(t) - \Delta R \cdot I(t) - V(t) \end{aligned} \tag{54}$$

Substituting (54) into (51), the final expression for $\dot{V}(t)$ is obtained as an explicit function of the following quantities:

- the unknown quantities to be identified: Q_{batt}, ΔR and $SOC(0)$

- the known model parameters α, β, R_0, R_1, C_1

- battery current I(t) and its time derivative $\dot{I}(t)$

- battery measured voltage $V(t)$ and its time derivative $\dot{V}(t)$.

Similarly to the procedure shown in the previous section, (51) can be rearranged in a way to separate unknown quantities to known quantities so to write (51) in the form:

$$W_g(t) = A_g(t) \cdot p_g \tag{55}$$

where the subscript g refers to the generalised method presented in this section. The quantities in (55) are described in the following:

- p_g is the vector of the three unknown quantities to be estimated:

$$p_g = \begin{bmatrix} SOC(0) \\ \dfrac{1}{Q_{batt}} \\ \Delta R \end{bmatrix} \tag{56}$$

  where all the components are taken as constant over the estimation time window.

- $W_g(t)$ is a scalar known function of measured quantities, defined as:

$$W_g(t) = \dot{V}(t) + \frac{V(t)}{R_1 C_1} + R_0 \dot{I}(t) + I(t)\left(\frac{R_0}{R_1 C_1} - \frac{1}{C_1}\right) - \frac{\alpha}{R_1 C_1} \tag{57}$$

- $A_g(t)$ is a vector of measured quantities which multiplies the vector pg of unknown parameters:

$$A_g(t) = \begin{bmatrix} \dfrac{\beta}{R_1 C_1} & -\dfrac{\beta}{R_1 C_1}\displaystyle\int_T I(\tau)d\tau - \beta I(t) & -\dot{I}(t) \end{bmatrix} \tag{58}$$

Starting from (55) and collecting measurements over an estimation time window of length $n \geq 3$, it is possible to build the matrices:

$$[W_g(t)] = \begin{bmatrix} W_g(t_1) \\ W_g(t_2) \\ \dots \\ W_g(t_n) \end{bmatrix}; [A_g(t)] = \begin{bmatrix} A_g(t_1) \\ A_g(t_2) \\ \dots \\ A_g(t_n) \end{bmatrix} \tag{59}$$

where $t_1, t_2, \dots, t_n$ are the time instants of the estimation window.

The linear LSs problem here defined is solved following the same procedure used for the Q-estimation algorithm, and the vector of unknown parameters is thus evaluated as:

$$\hat{p}_g = \left([A_g(t)]^T [A_g(t)]\right)^{-1} [A_g(t)]^T [W_g(t)] \tag{60}$$

The estimated $S\hat{O}C(0)$ corresponds to the initial condition with reference to the first instant of the estimation window. Using this information together with the current integral $\displaystyle\int_T I(\tau)d\tau$ computed with the current measurements, it is possible to evaluate the SOC at each time instant. The other components of vector $\hat{p}_g$ are the estimated battery capacity $\hat{Q}_{batt}$ and the estimated resistance increment $\Delta\hat{R}$.

6 Conclusions and future work

In this work, BMS algorithms for battery *SOC* and *SOH* estimation have been proposed. A state space model of a Li-ion battery pack used for e-bikes application was identified and validated experimentally.

The *SOC* estimation problem was addressed using: EKF and its adaptive version, AEKF. These algorithms have been implemented in simulation and tested on experimental data, and the estimation results were compared. The choice of an adaptive law for the process noise covariance matrix shows improvements in estimation performance. In terms of estimation error, the EKF results are into 5% estimation error range, while with AEKF this range is reduced down to 1%.

A capacity estimation algorithm based on LS approach was proposed to obtain a capacity monitoring capability over the battery lifespan. This method uses the model state estimation performed with AEKF. A general framework for combined *SOC* and *SOH* estimation is also presented, where the aging parameters are estimated together with *SOC*. As future work, the algorithms designed in this paper will be implemented on a BMS and tested on-board of vehicle with the real-time measurements.

References

Anderson, B.D.O. and Moore, J.B. (1979) *Optimal Filtering*, Prentice-Hall, Englewood Cliffs, New Jersey.

Barbarisi, O., Vasca, F. and Glielmo, L. (2006) 'State of charge Kalman filter estimator for automotive batteries', *Control Engineering Practice*, Vol. 14, No. 3, pp.267–275, Advances in Automotive Control.

Baronti, F., Zamboni, W., Femia, N., Rahimi-Eichi, H., Roncella, R., Rosi, S., Saletti, R. and Chow, M-Y. (2013) 'Parameter identification of Li Po batteries in electric vehicles: a comparative study', in *2013 IEEE International Symposium on Industrial Electronics (ISIE)*, May, pp.1–7.

Benesty, J. and Chen, J. (2011) *Optimal Time-Domain Noise Reduction Filters: A Theoretical Study*, 1st ed., No. VII, p.1, Springer Briefs in Electrical and Computer Engineering, Springer.

Ceraolo, M. (2000) 'New dynamical models of lead-acid batteries', *IEEE Transactions on Power Systems*, November, Vol. 15, No. 4, pp.1184–1190.

Chang, W. (2013) 'The state of charge estimating methods for battery: a review', *ISRN Applied Mathematics*, Article ID 953792.

Charkhgard, M. and Farrokhi, M. (2010) 'State-of-charge estimation for lithium-ion batteries using neural networks and EKF', *IEEE Transactions on Industrial Electronics*, December, Vol. 57, No. 12, pp.4178–4187.

Chiasson, J. and Vairamohan, B. (2005) 'Estimating the state of charge of a battery', *IEEE Transactions on Control Systems Technology*, Vol. 13, No. 3, pp.465–470.

Chicago Electric Bicycles LLC [online] http://www.chicagoelectricbicycles.com (accessed 09/10/2014).

Coleman, M., Lee, C.K., Zhu, C. and Hurley, W.G. (2007) 'State-of-charge determination from EMF voltage estimation: using impedance, terminal voltage, and current for lead-acid and lithium-ion batteries', *IEEE Transactions on Industrial Electronics*, October, Vol. 54, No. 5, pp.2550–2557.

Di Domenico, D., Fiengo, G. and Stefanopoulou, A. (2008) 'Lithium-ion battery state of charge estimation with a Kalman filter based on a electrochemical model', in *CCA 2008, IEEE International Conference on Control Applications, 2008*, September, pp.702–707.

Ding, W., Wang, D.J. and Rizos, C. (2006) 'Stochastic modelling strategies in GPS/INS data fusion process', in *Symposium on GPS/GNSS*.

Fathabadi, V., Shahbazian, M., Salahshour, K. and Jargani, L. (2009) 'Comparison of adaptive Kalman filter methods in state estimation of a nonlinear system using asynchronous measurements', in *Proceedings of the World Congress on Engineering and Computer Science*, Vol. 2.

Gao, L., Liu, S. and Dougal, R.A. (2002) 'Dynamic lithium-ion battery model for system simulation', *IEEE Transactions on Components and Packaging Technologies*, September, Vol. 25, No. 3, pp.495–505.

Gomadam, P.M., Weidner, J.W., Dougal, R.A. and White, R.E. (2002) 'Mathematical modeling of lithium-ion and nickel battery systems', *Journal of Power Sources*, Vol. 110, No. 2, pp.267–284.

Gu, W.B. and Wang, C.Y. (2000) 'Thermal-electrochemical modeling of battery systems', *Journal of the Electrochemical Society*, Vol. 147, No. 8, pp.2910–2922.

Han, J., Kim, D. and Sunwoo, M. (2009) 'State-of-charge estimation of lead-acid batteries using an adaptive extended Kalman filter', *Journal of Power Sources*, Vol. 188, No. 2, pp.606–612.

He, H., Xiong, R., Zhang, X., Sun, F. and Fan, J. (2011) 'State-of-charge estimation of the lithium-ion battery using an adaptive extended Kalman filter based on an improved Thevenin model', *IEEE Transactions on Vehicular Technology*, May, Vol. 60, No. 4, pp.1461–1469.

Hide, C., Moore, T. and Smith, M. (2003) 'Adaptive Kalman filtering for low cost INS/GPS', *The Journal of Navigation*, Vol. 56, No. 1, pp.143–152.

Hide, C., Moore, T. and Smith, M. (2004) 'Adaptive Kalman filtering algorithms for integrating GPS and low cost INS', in *Position Location and Navigation Symposium, 2004, PLANS 2004*, April, pp.227–233.

Jetto, L., Longhi, S. and Venturini, G. (1999) 'Development and experimental validation of an adaptive extended Kalman filter for the localization of mobile robots', *IEEE Transactions on Robotics and Automation*, April, Vol. 15, No. 2, pp.219–229.

Kim, J. and Cho, B.H. (2011) 'State-of-charge estimation and state-of-health prediction of a Li-ion degraded battery based on an EKF combined with a per-unit system', *IEEE Transactions on Vehicular Technology*, November, Vol. 60, No. 9, pp.4249–4260.

Lam, L., Bauer, P. and Kelder, E. (2011) 'A practical circuit-based model for Li-ion battery cells in electric vehicle applications', in *Telecommunications Energy Conference (INTELEC), 2011 IEEE 33rd International*, October, pp.1–9.

Lee, S., Kim, J., Lee, J. and Cho, B.H. (2008) 'State-of-charge and capacity estimation of lithium-ion battery using a new open-circuit voltage versus state-of-charge', *Journal of Power Sources*, Vol. 185, No. 2, pp.1367–1373.

Lin, X., Perez, H.E., Mohan, S., Siegel, J.B., Stefanopoulou, A.G., Ding, Y. and Castanier, M.P. (2014) 'A lumped-parameter electro-thermal model for cylindrical batteries', *Journal of Power Sources*, 1 July, Vol. 257, pp.1–11, ISSN 0378-7753.

Mohamed, A.H. and Schwarz, K.P. (1999) 'Adaptive Kalman filtering for INS/GPS', *Journal of Geodesy*, Vol. 73, No. 4, pp.193–203.

Moss, P.L., Au, G., Plichta, E.J. and Zheng, J.P. (2008) 'An electrical circuit for modeling the dynamic response of Li-ion polymer batteries', *Journal of the Electrochemical Society*, Vol. 155, No. 12, pp.A986–A994.

Pang, S., Farrell, J., Du, J. and Barth, M. (2001) 'Battery state-of-charge estimation', in *American Control Conference, 2001, Proceedings of the 2001*, IEEE, Vol. 2, pp.1644–1649.

Piller, S., Perrin, M. and Jossen, A. (2001) 'Methods for state-of-charge determination and their applications', *Journal of Power Sources, Proceedings of the 22nd International Power Sources Symposium*, Vol. 96, No. 1, pp.113–120.

Plett, G.L. (2004a) 'Extended Kalman filtering for battery management systems of LiPB-based HEV battery packs: part 1. Background', *Journal of Power Sources*, Vol. 134, No. 2, pp.252–261.

Plett, G.L. (2004b) 'Extended Kalman filtering for battery management systems of LiPB-based HEV battery packs: part 2. Modeling and identification', *Journal of Power Sources*, Vol. 134, No. 2, pp.262–276.

Plett, G.L. (2004c) 'Extended Kalman filtering for battery management systems of LiPB-based HEV battery packs: part 3. State and parameter estimation', *Journal of Power Sources*, Vol. 134, No. 2, pp.277–292.

Remmlinger, J., Buchholz, M., Meiler, M., Bernreuter, P. and Dietmayer, K. (2011) 'State-of-health monitoring of lithium-ion batteries in electric vehicles by on-board internal resistance estimation', *Journal of Power Sources*, Vol. 196, No. 12, pp.5357–5363.

Rubagotti, M., Onori, S. and Rizzoni, G. (2009) 'Automotive battery prognostics using dual extended Kalman filter', in *ASME 2009 Dynamic Systems and Control Conference*, pp.257–263.

Taborelli, C. and Onori, S. (2014) 'State of charge estimation using extended Kalman filters for battery management system', in *2014 IEEE International Electric Vehicle Conference*, December.

Tremblay, O., Dessaint, L-A. and Dekkiche, A-I. (2007) 'A generic battery model for the dynamic simulation of hybrid electric vehicles', *Vehicle Power and Propulsion Conference, VPPC 2007*, 9–12 September, IEEE, pp.284, 289.

Vasebi, A., Partovibakhsh, M. and Taghi Bathaee, S.M. (2007) 'A novel combined battery model for state-of-charge estimation in lead-acid batteries based on extended Kalman filter for hybrid electric vehicle applications', *Journal of Power Sources*, Vol. 174, No. 1, pp.30–40.

Welch, G. and Bishop, G. (1995) *An Introduction to the Kalman Filter*, University of North Carolina at Chapel Hill, Chapel Hill, NC, USA.

Zhang, S.S., Xu, K. and Jow, T.R. (2004) 'Electrochemical impedance study on the low temperature of Li-ion batteries', *Electrochimica Acta*, Vol. 49, No. 7, pp.1057–1061.

Notes

1   AllCell Technologies designs and manufactures lithium-ion battery packs for transportation and renewable energy applications. The company patented a thermal management technology based on phase change materials, which guarantees heat extraction and an uniform temperature distribution inside the pack. AllCell designs and produces the hardware and software component of BMS. AllCell Technologies LLC is located at 2321 W. 41st St. Chicago, IL 60609 USA.

2   A rate of $C/5$ correspond to a constant current value able to discharge the battery in 5 hours; $2C$ is the current corresponding to the double of the capacity, at which the battery is discharged at 1/2 hours.

3   The constant current-constant voltage (CC-CV) protocol was used to charge the battery: the battery is charged at a constant current ($1C$) until the voltage reaches the upper voltage limit, followed by a phase where voltage is hold at constant value until the current drops to zero.

4   This parameter is estimated in order to verify the accuracy of the battery pack capacity value, calculated in Subsection 2.1 using the value indicated by constructor for a cell at BOL.

5   RMS value of a generic vector $x(n)$ is defined as $\sqrt{\frac{1}{N}\sum_{n=1}^{N}|x(n)|^2}$ where N is the number of elements in vector $x(n)$.